Combustion, Explosion, and Shock Waves, Vol. 44, No. 6, pp. 639–654, 2008

HMX Flame Structure for Combustion in Air at a Pressure of 1 atm

A. A. Paletsky,[1] E. N. Volkov,[1] and O. P. Korobeinichev[1]

UDC 662.612+543.51

Translated from *Fizika Goreniya i Vzryva*, Vol. 44, No. 6, pp. 26–43, November–December, 2008.
Original article submitted September 10, 2007; revision submitted February 14, 2008.

The chemical structure of HMX flame during combustion in air at a pressure of 1 atm was calculated using molecular beam mass spectrometric sampling. HMX vapor was recorded for the first time near the burning surface. A total of 11 species were identified in the HMX flame (H_2, H_2O, HCN, N_2, CO, CH_2O, NO, N_2O, CO_2, NO_2, and HMX vapor), and their concentration profiles were measured. The HMX combustion was unstable. The species concentration profiles exhibit periodic pulsations related to variation in the HMX burning rate. The HMX flame structure at various distances to the burning surface was determined using the average value of the burning rate. Two main zones of chemical reactions in the flame were found. In the first zone ≈0.8 mm wide adjacent to the burning surface, HMX vapor decomposes and NO_2, N_2O, and CH_2O react with each other to form HCN and NO. In the second zone ≈0.8–1.5 mm wide, HCN was oxidized by nitric oxide to form the final combustion products. The composition of the final combustion products was analyzed. The global reaction of HMX gasification at a pressure of 1 atm was established. Heat release values in the condensed phase calculated by the global gasification reaction and by the equation of heat balance on the burning surface (using literature data from microthermocouple measurements) were analyzed and compared.

Key words: flame structure, HMX, molecular beam mass spectrometric sampling.

INTRODUCTION

Experimental studies of the flame structure of energetic materials play a very important role in the solution of the fundamental research problem of constructing a model for the combustion of condensed material. This paper deals with the chemical structure of HMX flame ($C_4H_8N_8O_8$). The study was performed at an air pressure $p = 1$ atm. The HMX flame structure has been studied previously by various methods [1–13] but it is still insufficiently understood. In particular, model concepts on the mechanism of HMX combustion [14, 15] assume the presence of HMX vapor (HMX_v) in the gas phase but available experimental data neither support nor refute the presence of the vapor in the flame.

In many papers, it is noted that, a pressure of 1 atm is the limit for stable combustion of HMX. Experimental evidence for unstable HMX combustion at $p = 1$ atm has been obtained in a number of studies [4, 6, 9, 16, 17] using various methods. This considerably complicates the analysis of this process.

Studies of the HMX flame structure using molecular beam mass spectrometry (MBMS) are described in [1, 2]. During HMX combustion at an argon pressure of 1 atm, fluctuations in the peak intensities of the combustion products have not been found. In those studies, only intensity profiles of the mass peak of the main combustion products at $m/e = 2$, 18, 27, 28, 29, 30, 42, 44, 46, and 75 were obtained but species concentrations were not determined. The zone adjacent to the burning surface where mass peak 75 (a characteristic fragmentation peak in the mass spectrum of HMX vapor) was a few tens of micrometers wide. The mass peak at

[1]Institute of Chemical Kinetics and Combustion, Siberian Division, Russian Academy of Sciences, Novosibirsk 630090; korobein@kinetics.nsc.ru.

$m/e = 42$ was identified as the molecular diaziridine ion (N_2CH_2). Unfortunately, in [1, 2], it was not possible to distinguish between HMX vapor in the gas phase and liquid HMX which was sucked into the probe and vaporized. The zone of consumption of formaldehyde and nitrogen dioxide identified by mass peaks 29 (CH_2O) and 46 (NO_2) was ≈0.6 mm wide, and the intensity of the mass peak at $m/e = 27$ (HCN) at this site was maximal and decreased to zero at a distance of ≈1.2 mm. Thus, it has been found that, in the HMX flame, as well as in the RDX flame, there are two zones of chemical transformations. It should be noted that, in MBMS studies [3] with a pressure decrease to 0.5 atm, it has been established from fluctuations in the peak intensities of the main combustion products that the HMX combustion is not stable and proceeds with a pulsation frequency of 1–10 Hz. The amplitude of the fluctuations in the intensities of the mass peaks at $m/e = 27$ (HCN) and $m/e = 30$ (NO) was significant — 30–40% of the maximum peak intensity.

The thermal structure of the HMX flame at pressures of 0.5–500 atm (at various initial temperatures) has been investigated by the microthermocouple method [4–6]. In [4, 5], WRe(5%)–WRe(20%) ribbon thermocouples 3–5 and 2–7 μm thick, respectively, were used. Pulsations of ±200 K were observed in the HMX flame temperature profile at a pressure of 0.5–1 atm. In [4, 6], the pulsations were attributed to the formation of bubbles of size 0.05–0.1 mm in the molten HMX layer [18]. An analysis of individual temperature profiles shows that the frequency of the flame temperature fluctuations is different and close to 15 Hz [4] near the burning surface (up to 0.15 mm) and to 3.5–4 Hz [6] at a distance of 0.2–0.7 mm from the burning surface. The values of heat release in the condensed phase calculated in [4–6] were negative: −14 cal/g [4], −41 cal/g [5], and −4.5 cal/g [6], respectively. It should be noted that, in those studies, the phase transition of HMX from the β to the δ-modification was ignored. It is evident that, with other parameters being close, the heat release values calculated in [5, 6] differ significantly. This is attributed to the fact that the heat release in the condensed phase due to chemical reactions calculated by the equation of heat balance on the burning surface is the sum of positive and negative quantities. The difference in the values of the heat fluxes from the gas phase due to radiation (30 cal/g [5], 7 cal/g [6]) and the surface temperature gradients ($7 \cdot 10^6$ K/m [5] and $8 \cdot 10^6$ K/m [6]) included in the heat-balance equation leads to significant differences in calculations of the heat release in the condensed phase. A formula for estimating the fraction of HMX decomposed in the condensed phase using the heat release is given in [5]. According to this formula, the heat release at a fixed pressure is determined as the fraction of the maximum possible heat release (at high pressures), which is proportional to the fraction of decomposed HMX (η) taking into account the heat consumed in the evaporation of undecomposed HMX ($1 - \eta$). Thus, the proposed estimate is based on the assumption that the condensed-phase HMX decomposition reaction does not change with increasing pressure. This can be the main cause of the error in estimating the fraction of the decomposed vapor. According to this estimate, the fraction of HMX decomposed in the condensed phase, was 0.17 and 0.26, respectively, because of the different heat release at $p = 1$ atm and the maximum heat release at $p = 500$ atm (−41 and 160 cal/g [5]; −4.5 and 230 cal/g [6]). Thus, in the gas phase near the burning surface, the fraction of HMX vapor in the gasification products can be estimated to be 0.83 and 0.74, respectively. The calculated stability parameter (k) of HMX combustion at pressures of 1–5 atm, which is equal to 0.62 at an initial sample temperature of 293 K, indicates the relative combustion stability [5]. In [6], it is specified that stable HMX combustion without periodic pulsations of temperature and velocity was observed at $p > 2$ atm, and at subatmospheric and atmospheric pressures, the temperature profiles was of a pulsating nature.

An unstable process of HMX combustion is reported in [7], where the HMX flame shape at pressures above atmospheric pressure (1.8–3 atm) was video recorded. The thermal flame structure at atmospheric pressure has not been investigated. The temperature in the condensed HMX layer, defined as the decomposition temperature at $p \approx 1.5$ atm was equal to ≈700 K. This value is slightly lower than the surface temperature (according to the schematic temperature profile given in [7]).

Close data on the surface temperature of HMX (with an additive of 3% paraffin) at a pressure of 1 atm are given in [14] — the temperature was equal to 690 K. At a pressure of 0.7 atm [19], the temperature profile showed pulsations with an amplitude of ≈100 K and a frequency of ≈0.5 Hz, indicating instability of HMX combustion at this pressure. In the study, round Pt–PtRh thermocouples of diameter 2.5 and 25 μm were used. The burning rate of HMX doped with 3% paraffin at $p = 1$ atm was 0.3 mm/sec.

In [16, 17], using a reactive force transducer, it was shown that HMX doped with 0.5% fine carbon particles is capable of burning in a pronounced self-oscillatory regime not only at $p = 0.5$ atm but also at $p = 1$ atm. At an initial sample temperature of 293 K, the pulsation frequency was 4.5–6 Hz, which is close to the data of [6]. The samples were ignited by laser radia-

TABLE 1

Nature (Existence of Pulsations) and Combustion Characteristics of HMX Samples at a Pressure of 1 atm

Method	T_s, K	T_f, K	Pulsations	r_b, mm/sec	ρ_s, g/cm^3	Gas	Shape and size of samples, mm	Purity
MBMS [1, 2]	—	—	No	0.45	1.76	Ar	Cylindrical (⌀ 10)	Not specified
Microthermocouple [4]	633	1873 or 2173	Present	0.35	1.7	N_2	Rectangular (length 12, width 7, height 5)	Not specified
Microthermocouple [5]	593 ±32	2393	—	0.41	1.7	N_2	Rectangular ($15 \times 15 \times 10$)	Not specified
Microthermocouple [6]	585	2393	Present	0.41	1.7	N_2	Rectangular ($15 \times 15 \times 10$)	>99%
Analysis of the reactive force signal [16, 17]	—	—	Present	0.58; 0.65 ± 0.05	1.81	N_2	Cylindrical (length 6–8, ⌀ 8, 10, 16)	Not specified +0.5% of soot
Microthermocouple [8]	687 ±18	2 353	No	0.20–0.32	1.72	N_2	Cylindrical (⌀ 7)	Not specified
Optical spectroscopy [9, 11]	—	2900	Present	—	1.83	—	Cylindrical (⌀ 9.5)	Not specified

Notes. T_s is the burning surface temperature, T_f is the temperature of the final combustion products, r_b is the burning rate of the HMX sample, and ρ_s is the density of the sample; dash denotes that this parameter is not specified in the paper.

tion. The results of [16] indicate a self-oscillatory combustion regime recorded by the variation in the reactive force signal. In [16], using the effective temperature sensitivity of the steady-state burning rate (β), the parameter k was estimated to be smaller than 1 ($k \approx 0.6$), i.e., according to theory, velocity fluctuations should be absent. This is in contradiction to the observed self-oscillations of the reactive force signal. The authors attribute the discrepancy between theory and experiment to incorrect use of the averaged combustion parameters for the self-oscillatory type of combustion.

Data on the physical parameters of the combustion wave of nitramines, including HMX, over a wide pressure range are collected in [20]. The authors of that paper suggest that the burning rate is affected by factors such as the degree of purity of HMX (presence of impurities), porosity (compaction pressure), sample diameter, composition of the ambient medium, and many other parameters.

In [8], an individual temperature profile of an HMX flame at a nitrogen pressure of 1 atm was obtained using ribbon WRe(5%)–WRe(20%) thermocouples 5–7 μm thick; the profile does not display appreciable temperature pulsations. It can be assumed that the combustion was stable.

As can be seen in Table 1, in most cases at a pressure of 1 atm, the HMX combustion was unstable. Since in all papers, except in [6], the purity of HMX is not specified, it is not possible to explain the different nature of HMX combustion from this point of view.

In some studies, the HMX flame structure at a pressure of 1 atm was investigated for CO_2 laser-assisted combustion [9, 10].

In [10], the HMX flame structure for laser-assisted combustion was studied using mass spectrometric microsampling. Concentration profiles were measured for ten basic species — H_2, H_2O, CH_2O, HCN, NO_2, N_2O, N_2, CO, CO_2, and NO. It was shown that CO_2 was absent near the burning surface. HMX vapor were not recorded. In addition, small amounts of HNCO, H_2NCHO, HONO, $C_3H_3N_3$ (triazine) were recorded near the burning surface. The front of the high-temperature zone of the HMX flame determined from the CN concentration profile in the same way as is done in [11] had a distinct dome-like shape form with an extended dark zone on the central axis of the sample. The width of the dark zone at atmospheric pressure was considerable — about 4.2 mm [12]. At a pressure of 1 atm, self-sustained HMX combustion [9] became unstable and aerosol particles were present near the burn-

ing surface, which made it impossible to measure the NO concentration. The maximum mole fractions of H_2CO and NO_2 determined near the burning surface were close to one another and were ≈0.065 each, and the OH concentration was about 0.036.

In [11], the final temperature of the HMX flame for self-sustained combustion in air was measured by the CN absorption spectrum using an optical method, and it was 2900 K. The error of this value is not discussed. The maximum measured mole fraction of NO was 0.22. The width of the flame zone at a pressure of ≈0.9 atm determined from the distance from the burning surface to the maximum peak intensity of CN was equal to ≈2 mm. For laser-assisted combustion, the HMX flame temperature at a distance of 6 mm from the burning surface was measured by the OH absorption spectrum with good accuracy and was 2772 ± 35 K. The calculated adiabatic temperature at $p = 1$ atm was 2922 K.

We note that the flames of energetic materials for laser-assisted combustion and for self-sustained combustion differ in structure, and it is therefore not correct to use experimental data on laser-assisted combustion of energetic materials to develop models for self-sustained combustion.

The composition of the products of thermal decomposition of HMX in argon (at $T = 673$ K) and in air (at $T = 623$ K) at atmospheric pressure was determined using Fourier spectroscopy combined with rapid heating [21]. A total of ten products wre recorded: CO, CO_2, NO, NO_2, N_2O, HCN, CH_2O, H_2O, HNCO, and HONO. The composition of the decomposition products depended weakly on the composition of the ambient medium. Nitrogen and hydrogen were not measured by this method. The Fourier spectroscopy technique combined with rapid heating of energetic materials to the burning-surface temperature is considered [21, 22] to be a suitable method for estimating the structure of the gasification products in the combustion wave at the surface temperature. However, it does not provide data on the decomposition kinetics.

The composition of the final combustion products of a HMX powder (≈1 g) at atmospheric pressure was determined using a mass spectrometric method in [23]. A total of seven species were recorded: N_2, CO, CO_2, H_2, NO, N_2O, and HCN. The total mole fraction of the last three species was less than 0.01. Water concentration was not measured in the experiments but was calculated from the material balance. The degree of HMX decomposition was 97.8%. The maximum deviation was obtained for hydrogen — 5%.

Thus, in the literature there is no consensus on the nature of HMX combustion at atmospheric pressure (steady-state or self-oscillatory) and, in addition, there is a significant spread in the data on the burning rate (0.2–0.65 mm/sec), surface temperature (585–687 K), and the final temperature (≈1873–2900 K). It should be noted that in the literature there are no data on HMX vapor concentration in the flame near the burning surface and on the chemical structure of the narrow zone adjacent to the burning surface.

The main objective of the present work was to perform a more comprehensive (than earlier) study of the chemical structure of the HMX flame for self-sustained combustion in air at a pressure of 1 atm. Great attention was given to the determination of the product composition at the burning surface, especially to the identification of HMX vapor and measurements of the vapor concentration.

EXPERIMENTAL TECHNIQUE

The HMX flame structure was studied using molecular beam mass-spectrometric sampling [3], which is one of the most informative method used to study the chemical structure of flames of energetic materials [24]. The essence of the experimental approach is that the burning sample moves to the probe at a velocity exceeding the burning velocity of the sample. The probe continuously takes samples at various distances from the burning surface, i.e., from various zones of the flame, up to the burning surface. Initially, the probe located at a significant distance from the burning surface (about 3–5 mm) samples the final combustion products from the high-temperature zone of the flame. Then, with decreasing distance between the probe and the burning surface, the probe samples intermediate combustion products from the low-temperature zone of the flame. The location of sampling can be determined with satisfactory accuracy by synchronizing measurements of the mass peak intensities and video recording of the distance between the probe and the burning surface (≈30–50 μm).

In the study, pressed HMX samples of density 1.80 ± 0.01 g/cm^3, diameter 8 mm, and length 6–8 mm were used; they were burned in air at a pressure of 1 atm (it was not possible to ignite the samples in an inert medium). The combustion was unstable, and periodic changes in the burning rate were recorded by processing a video record of the location of the burning surface. The average burning rate of the HMX samples was ≈0.65 mm/sec, the average velocity of motion of the probe to the burning surface was ≈0.6 mm/sec.

The lateral surface of the samples was coated with a thin layer of perfluorinated vacuum grease. During combustion, the central part of the sample protruded

relative to the lateral boundary, making it possible to observe the approach of the burning surface to the probe in transmitting light. The samples were ignited by an electrically heated Nichrome wire located at a distance of 0.5–1 mm from the sample surface. After ignition of the sample, the wire was removed from the flame. After the completion of the combustion, no remainder was observed on the substrate. The HMX flame structure was studied using an aluminum probe coated with a thin layer of Al_2O_3. The thickness of the probe wall was ≈70 μm, and the diameter of the entrance aperture was ≈70 μm. In each experiment, once the probe came in contact with the HMX burning surface, the probe aperture was plugged. The probe was removed and cleaned. The size of the aperture was checked under a microscope.

Mass peak intensities of the combustion products were measured using a data acquisition control system based on the CAMAC modules and a personal computer. Complete mass spectra in the range m/e = 35–83 were recorded using a LeCroy 9310 digital storage oscillograph. Combustion products were identified by mass spectra of individual species. N_2O and CO_2 were separated by the peak at $m/e = 22$ (CO_2^{++}), and of CO and N_2 by the peak at $m/e = 14$ (N^+) after taking into account the contributions to it from nitrogen-containing products (NO, N_2O, NO_2, and HCN). The quantitative content of species in a sample was determined using calibration coefficients. For most gases, the accuracy of the calibration coefficients was ±5% for H_2O, and for HCN, and NO_2, it was ±10%.

Detection and Quantitative Determination of HMX Vapor Concentration

To find and identify HMX vapor, we performed special experiments with HMX decomposition/vaporization in a flow reactor with argon at atmospheric pressure. The design of the reactor is described in [25]. The products were sampled using a preliminarily heated quartz probe with an aperture diameter of 100 μm. Additional heating of the probe was performed by a conical spiral from a Nichrome wire wound on the outside of the cone near the probe tip. The additional heating was performed to prevent HMX vapor condensation in the aperture and on the inner walls of the probe. In experiments without heating of the probe, the probe aperture was soon plugged, resulting in the disappearance of the signal. The temperature of the probe tip (≈573 K) was slightly higher than the HMX melting point (553 K). The velocity of the argon flow was 0.8–1.5 cm^3/sec (normal conditions). An acetone solution of HMX was applied onto the central part of a metal plate 0.1 mm thick which was used as a heater. During evaporation of acetone at room temperature, HMX crystals of size $\leqslant$40 μm were formed on the surface of the heater. The total mass of the HMX sample did not exceed 1 mg. The heater was placed at a distance of ≈1–2 mm from the probe aperture. The plate was heated by an electric current, and its temperature was measured by a Chromel–Coppel thermocouple of 50 μm diameter.

Mass spectra of HMX vapor at an ionization energy of 70 eV were obtained in a number of studies [26–29]. These data are presented in Table 2. The most complete mass spectrum of the vapor (intensities of 25 mass peaks in a range of m/e = 15–222) was obtained in [27] under effusion molecular beam conditions using a quadruple mass spectrometer. In [28], a mass spectrum of HMX vapor was measured in a range of masses beginning at $m/e = 46$. The data of [29] were obtained under molecular leak conditions and differ significantly from the results of [27] even in the main peak intensity and will not be discussed in the present paper. The above-mentioned differences in the ratio between the peak intensities in mass spectra depend on the method of introducing the analyzed sample to the mass spectrometer ion source. Since this ratio affects the accuracy of quantitative determination of the other species in the sample, in the present work we obtained a mass spectrum of HMX vapor that coincides within the measurements error with the mass spectra obtained in our previous study [26]. All mass spectra of HMX vapor are characterized by the absence of mass peak 44. This feature of the mass spectrum was used to determine the ratio between HMX vapor and its decomposition products under the conditions of our experiments. Since heating of HMX on the plate in the flow reactor results in the formation of not only HMX vapor but also its decomposition products, the experimental conditions (blowing velocity and heating rate) were chosen so that the intensity of mass peak 44 in the products was minimal, and hence, the amount of HMX vapor was larger than that of its decomposition products. Table 2 gives the mass spectra obtained in the present work in which mass peak 44 is not observed and the intensity of mass peak 42 is maximal. This agrees with the data of [27]. The differences in the intensities of mass peaks 30 and 75 are most likely due to differences in the experimental conditions, including the system for introducing samples to the mass spectrometer ion source.

The calibration coefficient for HMX vapor was determined by the formula $K_{\mathrm{HMX/Ar}} = \Delta I(75)_{\mathrm{HMX}}/\Delta I(40)_{\mathrm{Ar}}$, where $I(75)$ is the intensity of mass peak 75 characteristic of the mass spectrum of

TABLE 2
Mass Spectrum of HMX Vapor

Source	m/e				
	29	30	42	46	75
[26]; present work	15	71	100	62	37
[27]	14.7	25.5	100	65.4	51.4
[28]	—	—	—	100	26
[29]	—	65	25	100	10

HMX. The measured coefficient was 0.037. The accuracy of the calibration coefficient for HMX vapor was ±15%. The accuracy of determining the concentrations of N_2, CO, and NO was 5–10% and was the higher the greater the intensity of the measured signal. In calibration experiments for stable species, measurements were conducted for a long time to increase the accuracy of determination of the calibration coefficients. In addition, the calibration coefficient of stable species that are not condensed with decreasing temperature in the probe nozzle does not depend on the concentration of the calibrated gas in the carrier gas. Otherwise, (during formation of clusters in the supersonic jet behind the probe), the measured calibration coefficients could have exceeded their true values by an order of magnitude. In addition, the calibration coefficients begin to depend on species concentrations in the sample, which in turn, leads to incorrect quantitative measurements of species concentrations. These problems are solved primarily by reducing the species concentrations in the probe, reducing the flow rate of the analyzed sample through the probe by decreasing the diameter of the probe entrance aperture or by increasing the temperature of the carrier gas and/or the probe. All abovementioned problems are extremely urgent in calibration experiments for HMX vapor. At high rates of heating of the HMX sample, the process of its evaporation depended on the uniformity of application of the sample. For a small thickness of the sample applied onto the heater ribbon, the fraction of HMX vapor is large compared to the fraction of its decomposition products. In the preparation of a sample by crystallization of HMX from a solution, the total amount of the substance on the heater surface was checked, and the uniformity of application was not reproduced from experiment to experiment. Nonuniform application during evaporation led to an uncontrollable concentration of HMX vapor in the carrier gas flow. To prevent the formation of HMX clusters, the calibration coefficient for HMX vapor was determined at low intensities of the peak at $m/e = 75$, which was responsible for the low accuracy of its measurements.

Determining the calibration coefficient for nitramine vapor is an extremely difficult but very important problem for the correct determination of the gas-mixture composition near the HMX burning surface. Therefore, in the future, we are planning to perform additional calibration experiments to refine these values.

To choose the optimum conditions of experiments on production of HMX vapor, we studied the behavior of HMX samples heated on the plate in the flow reactor using video recording. The heating rate, the maximum temperature, and the blowing velocity were varied. At low velocities of the cold gas blowing over the plate and upon the attainment of a temperature of ≈573 K, the sample placed at the center of the plate melted and a large amount of long crystals 20–30 μm thick were formed in the gas phase. The latter resulted from condensation of HMX vapor from the gas phase. Video recording of the process was performed through a microscope. If the carrier gas was heated, the formation of the crystals was not observed, i.e., the entire HMX was evaporated.

RESULTS AND DISCUSSION

Figure 1 shows species concentration profiles in a HMX flame for combustion in air at a pressure of 1 atm versus time. The concentration values are given without corrections for the temperature and the hydrodynamic perturbations caused by the probe. Concentrations were measured for 11 species — H_2, H_2O, HCN, N_2, CO, CH_2O, NO, N_2O, CO_2, NO_2, and HMX vapor. The abscissa plots time reckoned in the reverse direction corresponding to the motion of the probe to the burning surface. The zero on the abscissa corresponds to the moment of contact of the probe with the burning surface. One can see periodic pulsations in the concentration profiles. The pulsations have a duration of 0.3–0.5 sec and appear at a frequency of ≈0.7 Hz. The first pulsation is manifested as an increase in the concentrations N_2O and HMX vapor in the time interval of 0.7–0.9 sec. Another three pulsations (t = 2–5 sec) are related to simultaneous increases in the HCN and NO concentration and a reduction in the CO and N_2 concentrations. An analysis of the video record showed that, after the time of 2.7 sec, the probe is in the luminous region of the flame. However, at the moment of occurrence of the pulsations observed at $t > 2.7$ sec, the luminosity of the flame under the probe decreases. The concentrations of HCN, NO, CO, and N_2 at these moments also correspond to the concentrations in the dark zone of the flame. According to the video record, at same moments, the burning rate increases

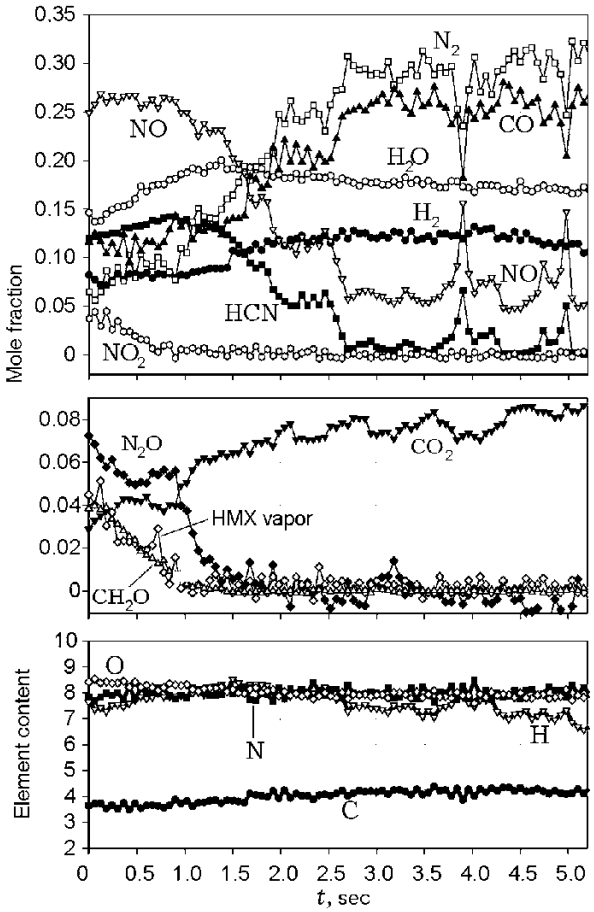

Fig. 1. Species concentration profiles in a HMX flame for combustion in air at a pressure of 1 atm versus time. Initial data.

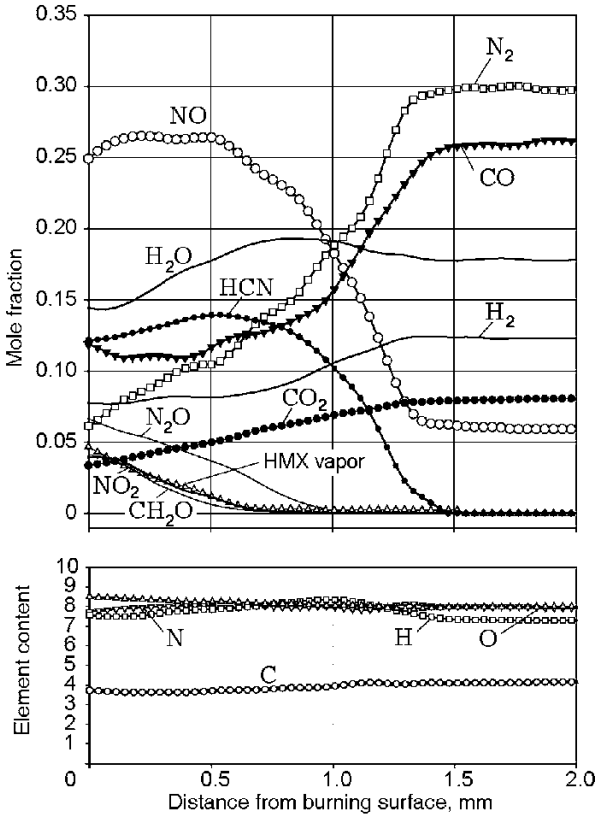

Fig. 2. HMX flame structure in air at a pressure of 1 atm. Averaged and smoothed profiles.

from ≈0.45 mm/sec (the value was determined in the time interval of 2.7–3.7 sec) to ≈0.8 mm/sec, resulting in an increase in the width of the flame zone (corresponds to the reduction in luminosity under the probe) and, as a consequence, in the occurrence of pulsations in the concentration profiles. The observed pulsations of the combustion products are in antiphase: the concentrations of HCN and NO increase simultaneously, and those of CO and N_2 decrease. It should be noted that significant changes (at the moment of pulsations) in species concentrations (up to 30% of the maximum value) did not affect the total element content over the flame zone.

Averaged profiles of species mole fractions in the HMX flame versus the distance to the burning surface are presented in Fig. 2. Averaging was performed by multiplying the current time by the average velocity of motion of the burning surface relative to the probe, which was equal to ≈0.6 mm/sec. The averaged flame structure will be discussed below.

The HMX flame at $p = 1$ atm has a two-zone structure. In the first zone at a distance up to ≈0.7 mm from the burning surface, consumption of HMX vapor, NO_2, and CH_2O and partial consumption of N_2O with the formation of H_2, H_2O, CO, N_2, CO_2, HCN, and NO take place. The zone of full consumption of N_2O (≈1 mm from the burning surface) is larger than the zone of consumption of HMX vapor (as well as in the RDX flame [30]). In the second zone of the flame at a distance of 0.8–1.5 mm from the burning surface, intense consumption of HCN and NO with the formation of the final combustion products N_2, CO, and H_2 takes place.

The widths of the first (≈0.7 mm) and the second (≈0.8 mm) zones of the HMX flame at a pressure of 1 atm are close to the widths of the intensity profiles of the corresponding peaks (≈0.6 and ≈0.6 mm) obtained in [1, 2]. The width of the flame zone [11] measured at a pressure below atmospheric pressure ($p \approx 0.9$ atm) is equal to ≈2 mm, which also agrees with our measurements (≈1.5 mm).

The composition of the products near the surface of self-sustained combustion at a pressure of 1 atm is

TABLE 3

Composition of the Products near the HMX Burning Surface at $p = 1$ atm in Comparison with Data [9] and Data on Laser-Assisted HMX Combustion [10], Thermal Decomposition [21], and Linear Pyrolysis [13]

Source	r_b, mm/sec	H_2	HCN	NO	N_2	CO	H_2O	CO_2	N_2O	NO_2	CH_2O	HMX_v
Present work	0.65	0.077	0.122	0.249	0.061	0.119	0.144	0.034	0.066	0.041	0.04	0.047
[10]	0.9	0.01	0.19	0.14	0.09	0.06	0.14	0	0.1	0.11	0.16	—
[13]	1	0.016	0.204	0.191	0.035	0.019	0.069	0.01	0.142	0.158	0.154	—
[21]	—	—	0.15	0.16	—	0.075	0.025	0.025	0.18	0.18	0.18	—
[9]	—	—	—	≈0.22	—	—	—	—	—	0.065	0.065	—

TABLE 4

Content of the Elements C, H, N, and O in the Products near the Burning Surface in the Thermal Decomposition Products of HMX

Source	C (4)	H (8)	N (8)	O (8)
Present work	3.72 (7%)	7.56 (5.5%)	7.73 (3.4%)	8.48 (6%)
[10]	4 (0%)	7.9 (1.3%)	6.8 (15%)	6.9 (13.8%)
[13]	3.5 (12.5%)	6.2 (22.5%)	6.8 (15%)	6.9 (13.8%)
[21]	3.7 (7.5%)	4.9 (38.8%)	5.8 (27.5%)	7.4 (7.5%)

Note. The deviation from the initial element content is given in parentheses.

given in Table 3 in comparison with data [10] where laser-assisted HMX combustion was studied and data [13, 21] on thermal decomposition and linear pyrolysis. In papers [9, 10, 13, 21], whose results are presented in Table 3, no information is given on HMX vapor in the decomposition products. In our case, the mass fraction of HMX vapor near the burning surface is 35%. From an analysis of the element content in the combustion products or decomposition in comparison with the initial amount [C (4), H (8), N (8), and O (8)], the maximum deviation from the initial value in our case (the first line in Table 4) is observed for C — about 7%. In [10, 13, 21], the maximum deviations for the other elements were 15% or more. Thus, in our study, the composition of the products near the HMX burning surface at a pressure of 1 atm was determined more fully and correctly than available literature data.

According to [15, 31, 32], the condensed-phase decomposition of HMX (HMX_l) occurs by two pathways, depending on the heating rate:

$$HMX_l \Rightarrow 4CH_2O + 4N_2O, \quad \text{(R1)}$$

$$HMX_l \Rightarrow 4HCN + 2(NO_2 + NO + H_2O). \quad \text{(R2)}$$

At low heating rates (R1), the exothermic reaction with the formation of CH_2O and N_2O dominates. The other pathway of HMX decomposition (R2) proceeds mainly at high heating rate and is an endothermic reaction involving the formation of NO_2, HCN, H_2O, and NO.

The most important secondary reactions in the condensed phase is the reaction between CH_2O and NO_2 resulting in the formation of CO, NO, and H_2O:

$$CH_2O + NO_2 \Rightarrow CO + NO + H_2O. \quad \text{(R3)}$$

This reaction can proceed in bubbles. The primary reactions (R1) and (R2) can also proceed in the gas phase with the participation of HMX vapor. As the bubbles reach from the burning surface, HMX vapor together with the products are ejected into the gas phase. Thus, along with HMX evaporation into the gas phase from the burning surface, it is also evaporated in the bubbles present in the condensed phase:

$$HMX_l \Leftrightarrow HMX_v. \quad \text{(R4)}$$

The concentration of the HMX decomposition products in laser-assisted combustion is several times higher than that in self-sustained combustion: 1.5 times for N_2O, 4 times for CH_2O, 2.7 times for NO_2, and 1.5 times for HCN, and the concentrations of NO, CO, and H_2O are lower. Mole fractions of NO (≈0.22), NO_2 (0.065), and CH_2O (0.065) close to our measurements (≈0.25 and ≈0.04) for self-sustained combustion were obtained in [9] using an optical method (see Table 3). It can be assumed that this ratio between the concentrations of the products of gasification according to reactions (R1)–(R3) considered above is related to the more complete laser-assisted decomposition of HMX during

combustion. This effect, however, can also be related to HMX decomposition on the walls of the probe [10] in the molecular leak mode.

Data on the composition of the HMX decomposition products during linear pyrolysis in vacuum [13] and high-velocity heating in air [21] are close to data for laser-assisted combustion [10] but differ from data for self-sustained HMX combustion.

The amount of HMX vapor in the products of its gasification during combustion is one of the key parameters in nitramine combustion theory, which has not yet been determined by direct methods.

For example, in [10], to obtain the best agreement between modeling results and experimental data on the HMX flame structure for laser-assisted combustion, it was postulated that the products near the surface contain 10–50% HMX vapor. In [15], it is reported that, according to the combustion model considered, HMX evaporation is an important factor at all pressures. The HMX burning surface temperature calculated according to the model of [15] in the pressure range 1–70 atm well describes experimental values [4]. It was found that at a pressure of 1 atm and a surface temperature of 633 K [4], about 52% of HMX is evaporated to the gas phase [15]. According to this model, the amount of HMX vapor increases with a pressure rise, which, however, contradicts the results [5] obtained under the assumption that, at high pressures, HMX is entirely decomposed in the condensed phase.

The composition of the final products of HMX combustion at $p = 1$ atm is close, but not identical, to that in thermodynamic equilibrium since it contains $\approx$0.06 mole fraction of NO (line 5 in Table 5). Table 5 gives the results of thermodynamic calculations of the combustion-product composition and adiabatic temperature at a pressure of 1 atm for two different values of the enthalpy of formation of HMX.

The composition of the final combustion products in the experiment was determined at a distance 2–3 mm from the burning surface. At these distances, the flame is one-dimensional and the height of the cone of mixing of the combustion products with the products formed at the edges is much higher than the total width of the flame at a sample diameter 8 mm. Therefore, at a distance of 2–3 mm, admixture of the products that reacted with ambient air does not affect the oxygen and nitrogen contents compared to the initial amounts.

The thermodynamically equilibrium composition and the temperature of the combustion products calculated for various enthalpies of formation of HMX change only slightly. It should be noted that in the literature there are different values for the enthalpy of formation of solid HMX, but an analysis [35] has shown that the only value measured experimentally is the value of 71 cal/g obtained in [34] and we use it in the present work. Although the data of [23] (see line 6 in Table 5) are close to the thermodynamic equilibrium composition but they are characterized by a number of drawbacks: the amount of water was not measured but was calculated from the material balance, and the low content of NO [23] compared to our data (see line 5 in Table 5) is most likely related to an indirect analysis of samples.

The experimentally measured concentration of OH radicals [9] for HMX combustion (0.036 mole fraction) exceeds the thermodynamically equilibrium value (0.026) and was not used for corrections of our experimental composition. This excess may be related to the measurement error of the spectroscopic method used in [9].

The presence of NO in the final products indicates that the combustion is incomplete, and, hence, the temperature value can be expected to be lower than the thermodynamically equilibrium value. Using the value of [34] for the enthalpy of formation of HMX and the composition of the final combustion products supplemented by the equilibrium concentrations of H and OH radicals (see line 4 in Table 5), we estimated the temperature of the gas mixture to be equal to 2710 K (line 4 in Table 5,). The estimate was obtained by considering only the main radicals with a mole fraction larger than 0.01. The deviation of the element content in the final combustion products from the initial values (see line 4 in Table 5) does not exceed 3%. The adiabatic temperature and the thermodynamically equilibrium composition was calculated using the EQUIL code from the CHEMKIN software [36]; the initial conditions were the estimated temperature and experimental composition given in line 4 in Table 5. The result of the calculation is presented in the third line of the same table. It is evident that NO content decreased by an order of magnitude, and the temperature and composition of the combustion products are close to the calculated thermodynamically equilibrium condition (see line 2 in Table 4). Thus, the analysis of the experimentally measured composition of the HMX combustion products at $p = 1$ atm shows that the final temperature in the HMX flame does not reach the adiabatic value (2925 K) and is equal to 2710 K and the NO concentration is several times the adiabatic value. The estimated temperature of the final products of HMX combustion (2710 K) is $\approx$320 K higher than the experimental values obtained using tungsten–rhenium thermocouples [6], is 190 K lower than the temperature measured from the emission spectra of CN using an optical method, and agrees reasonably well with the HMX flame tempera-

TABLE 5

Composition of the Final Products of HMX Combustion at $p = 1$ atm

No.	T, K	N_2	CO	H_2O	CO_2	H_2	NO	H	OH
1	2918	0.316	0.244	0.197	0.074	0.089	0.004	0.037	0.025
2	2925	0.316	0.244	0.196	0.073	0.089	0.005	0.038	0.026
3	2959	0.308	0.251	0.206	0.071	0.08	0.005	0.039	0.025
4	2710	0.279	0.244	0.167	0.075	0.115	0.056	0.038*	0.026*
5	—	0.298	0.26	0.178	0.08	0.123	0.06	—	—
6	—	0.332	0.238	0.228	0.098	0.092	0.008	—	—

Notes. Composition Nos. 1 and 2 were obtained by thermodynamic calculations using the ASTRA code for ΔH_f^0(HMX) = 60.5 cal/g [33] and 71 cal/g [34, 35], respectively, composition No. 3 was obtained by thermodynamic calculations using the EQUIL code under initial conditions 4, No. 4 is the experimentally measured composition of the final combustion products supplemented by equilibrium concentrations of H and OH radicals (the values marked by an asterisk were obtained at $T = 2925$ K; $T = 2710$ is a temperature estimate), No. 5 is the by experimentally measured composition of the final combustion products, and No. 6 is obtained by combustion in a closed volume [23]).

ture in laser-assisted combustion (2772 K) measured at good accuracy from absorption spectra of OH [11].

It is known that tungsten–rhenium thermocouples are suitable for use in oxidizing media [37]. It should be noted that, near the burning surface (at $T \approx 1273$–1773 K) there is a significant amount of NO (maximum mole fraction ≈0.25), which also remains in the final products at a temperature of ≈2710 K. The lower final temperatures of the HMX flame compared to those measured by an optical method can be attributed to incorrect use of thermocouples of this type.

Calculation of the Composition of the Gasification Products of HMX and Heat Release in the Reaction Layer of Condensed-Phase HMX

The stoichiometric coefficients (ν_i) of the global reaction of HMX gasification (HMX $\rightarrow \sum \nu_i B_i$) can be calculated knowing the mass fluxes of the species on the burning surface. A more detailed description of this procedure is given in [30]. The stoichiometric coefficient of the ith species is determined as the ratio of the mass flux of the ith species on the burning surface to the flux of HMX. The total mass flux of the ith species in dimensionless form (G_i) with the diffusion and thermal diffusion taken into account can be written as

$$G_i = \frac{M_i}{M}\left(x_i - \frac{D_{im}}{v}\frac{dx_i}{dz}\right) - \frac{1}{\rho v}\frac{D_i^T}{T}\frac{dT}{dz}.$$

Here M_i and x_i are the molecular weight and mole fraction of the ith species, M is the average molecular weight of the species, D_{im} is the mixture diffusion coefficient of the ith species, D_i^T is the thermal-diffusion coefficient of the ith species, v is the velocity of the species flux, $\dfrac{dx}{dz}$ is the concentration gradient of the ith species, and ρ is the density of the species.

From the formula, it is evident that to calculate the species mass flux on the burning surface, it is necessary to know the burning-surface temperature T_s and the gas-phase temperature gradient $\dfrac{dT}{dz}$ near the burning surface. As was shown in the introduction, the values of these quantities measured at $p = 1$ atm in various studies [4–6, 8] vary widely. Therefore, the calculations of the global reaction of HMX gasification at $p = 1$ atm were performed for three values of T_s and their corresponding values of the temperature gradient: $T_s = 687$ K ($dT/dz = 3.55 \cdot 10^6$ K/m) [8], 633 ($dT/dz = 4 \cdot 10^6$ K/m) [4], and 593 K ($dT/dz = 7 \cdot 10^6$ K/m) [5]. In the calculations, we used the species concentration gradients determined from smoothed concentration profiles (see Fig. 2).

Table 6 gives the experimentally measured composition of the products near the HMX burning surface at $p = 1$ atm and three compositions of the gasification products obtained from the experimentally measured composition of the products. Since, near the burning surface, the species concentrations change only slightly (See Fig. 2), the changes in the product composition due to diffusion are not significant. Accounting for thermal diffusion has a significant influence only on the hydrogen concentration. Apart from hydrogen, a marked change in the absolute concentration is observed for NO, which

TABLE 6

Composition of the Gasification Products (in Mole Fractions) near the HMX Burning Surface at $p = 1$ atm

No.	H_2	H_2O	HCN	N_2	CO	CH_2O	NO	CO_2	N_2O	HMX_v	NO_2	C/H/O/N
1	0.077	0.144	0.122	0.061	0.119	0.040	0.249	0.034	0.066	0.047	0.041	3.72/7.56/8.48/7.73
2	0.097	0.145	0.119	0.055	0.121	0.039	0.238	0.032	0.067	0.046	0.041	3.74/7.95/8.51/7.65
3	0.099	0.145	0.119	0.055	0.121	0.039	0.238	0.032	0.067	0.045	0.041	3.74/7.98/8.50/7.65
4	0.114	0.143	0.117	0.055	0.119	0.038	0.235	0.031	0.065	0.043	0.039	3.74/8.24/8.50/7.64

Notes. No. 1 is the experimental composition of the products and Nos. 2, 3, and 3 are the compositions of the gasification products calculated at $T_s = 687$ K ($dT/dz = 3.55 \cdot 10^6$ K/m) [8], 633 ($dT/dz = 4 \cdot 10^6$ K/m) [4], and 593 K ($dT/dz = 7 \cdot 10^6$ K/m) [5], respectively.

TABLE 7

Heat Release in the Reaction Layer of the Condensed Phase during HMX Combustion Calculated Using Various Data on $c_p(T)$

Source of data on $c_p(T)$	Q, cal/g		
	Composition No. 2 ($T_s = 687$ K [8])	Composition No. 3 ($T_s = 633$ K [4])	Composition No. 4 ($T_s = 593$ K [5])
[41]	212.4	205.0	203.0
[35]	112.9	119.8	126.6

Note. Compositions of the gasification products are presented in Table 5.

is due to its high concentration. The relative change in the NO concentration in this case is ≈5%.

It is evident that composition Nos. 2 and 3 calculated for very close temperatures gradients but different surface temperatures are almost identical. Additional calculations for even more greatly different temperatures of the burning surface (593 and 687 K) but with identical temperature gradients have shown that the calculated compositions also coincide. That is, in this case, the spread in the values of the burning surface temperature does not significantly influences the result of calculation of the gasification product composition. The spread in the values of the temperature gradient is much greater (the maximum and minimum values differ by a factor of almost two); therefore, the absolute value of the temperature gradient has a more significant effect on the composition of the gasification products.

Table 6 also gives the element content ratios for all compositions. Generally, accounting for diffusion and thermal diffusion slightly improves the element balance. The maximum deviation of the element content from the initial value observed for element C is only 6.5%.

For composition No. 3 from Table 6, the HMX gasification at a pressure of 1 atm is described by the following reaction:

$$\mathrm{HMX} \to 1.817\mathrm{NO} + 1.103\mathrm{H_2O} + 0.919\mathrm{CO} + 0.905\mathrm{HCN} + 0.757\mathrm{H_2} + 0.508\mathrm{N_2O} + 0.421\mathrm{N_2} + 0.345\mathrm{HMX}_v + 0.309\mathrm{NO_2} + 0.240\mathrm{CO_2} + 0.298\mathrm{CH_2O}.$$

Knowing the stoichiometric coefficients of the global reaction of gasification (ν_i), it is possible to calculate the heat release on the burning surface:

$$Q = -\Delta H_{T=T_s} = H(\mathrm{HMX}_l)_{T=T_s} - \sum \nu_i H(B_i)_{T=T_s},$$

$$H(\mathrm{HMX}_l)_{T=T_s} = \Delta_f H^0(\mathrm{HMX}_\beta) + \int_{T_0}^{T_{\beta\to\delta}} c_{p,\mathrm{HMX}_\beta}(T)dT + q_{\beta\to\delta} + d + \int_{T_{\beta\to\delta}}^{T_{\delta\to l}} c_{p,\mathrm{HMX}_\delta}(T)dT + q_{\delta\to l} + \int_{T_{\delta\to l}}^{T_s} c_{p,\mathrm{HMX}_l}(T)dT.$$

where $T_{\beta\to\delta}$ and $q_{\beta\to\delta}$ are the temperature and heat of phase transition of the β-modification to the δ-modification, $T_{\delta\to l}$ and $q_{\delta\to l}$ are the temperature and heat of melting of the δ-modification of HMX, and c_p is the specific heat capacity at constant pressure.

HMX can exist in four crystal modifications. The β-modification of HMX (β-HMX) is the most stable under normal conditions. During heating in a combustion wave, the β-modification of HMX is transformed to the

TABLE 8

Heat Release in the Reaction Layer of the Condensed Phase during HMX Combustion Calculated by the Heat-Balance Equation

T_s, K	$\frac{dT}{dz}$, 10^6 K/m	m, g/(cm$^2\cdot$sec)	λ_g, 10^{-4} cal/(cm$\cdot$sec$\cdot$K)	Q, cal/g	
				$c_p(T)$ from [41]	$c_p(T)$ from [35]
687	3.55	0.045 [8]	1.54	89	−10
633	4	0.0595 [4]	1.42	89	4
593	7	0.07 [5]	1.33	33	−43

δ-modification. According to [38], this phase transition occurs at $T_{\beta\to\delta} = 460$ K. Further heating leads to melting of the δ-modification of HMX ($T_{\delta\to l} = 551$ K [38]).

In the calculations, we used the following values for the enthalpy of formation of HMX and phase-transition heat: $\Delta_f H^0$(HMX) = 87.9 kJ/mole [34], $q_{\beta\to\delta} = 9.8$ kJ/mole [34], and $q_{\delta\to l} = 69.9$ kJ/mole [39].

Figure 3 shows the temperature dependence of the specific heat capacity of HMX according to different authors [5, 34, 35, 40, 41]. In [4, 6], the temperature dependence of the heat capacity of the condensed phase is ignored and its constant value is used: 0.3 cal/(g$\cdot$K) in [4] and 0.36 cal/(g$\cdot$K) in [6]. In [5], the temperature dependence of the heat capacity of the condensed phases is introduced but the dependence differs greatly from the data of the other authors (see Fig. 3). Of the results presented in the figure, the experimentally measured data are those obtained in [34, 40, 41]. From the figure, it is evident that the data of [40] and [41] for β-HMX coincide with very good accuracy. The dependence for β-HMX obtained in [34] is also close to the data of [40, 41]. A unified temperature dependence of the heat capacity for β- and δ-HMX is given in [41]. In the case of δ-HMX, the difference between the data of [34] and [41] is more significant than for β-HMX, but with increasing temperature, this difference decreases, and at $T > T_{\beta\to\delta} = 460$ K, it is less than 10%. In [35], temperature dependences of the heat capacity were calculated for solid (β- and δ-modifications) and liquid HMX. However, the values obtained for β- and δ-HMX turned out to be lower than experimental data; in [35], it is noted that the experimental data are apparently more reliable.

To evaluate how the choice of the temperature dependence of the heat capacity of HMX can affect the result of calculation of the heat release in the condensed phase, in our calculations we used the data of [41] and [35]. In [41], a temperature dependence of the heat capacity for liquid HMX is absent; therefore, for liquid HMX, we used the same dependence as for solid HMX.

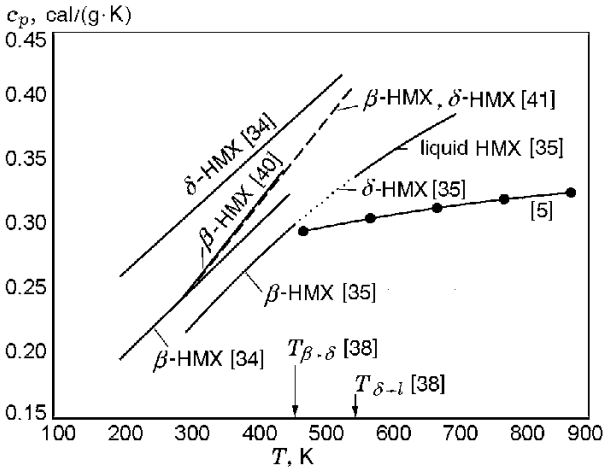

Fig. 3. Temperature dependence of the heat capacity of HMX according to data of different authors.

For each composition of the gasification products of HMX from Table 6, the heat release Q on the burning surface was calculated. The calculation results are presented in Table 7. It is evident that the choice of the temperature dependence of the heat capacity for HMX has a strong effect on the calculation result: the difference between the values of Q can reach 100 cal/g (composition No. 2). Variation in the burning surface temperature has a much weaker effect on the value of Q.

The heat release on the burning surface can also be calculated by the equation of heat balance on the burning surface:

$$Q = \int_{T_0}^{T_{\beta\to\delta}} c_{p,\mathrm{HMX}_\beta}(T)dT + q_{\beta\to\delta}$$

$$+ \int_{T_{\beta\to\delta}}^{T_{\delta\to l}} c_{p,\mathrm{HMX}_\delta}(T)dT + q_{\delta\to l}$$

TABLE 9

Difference between the Heat Release Values in the Reaction Layer of the Condensed Phase (ΔQ) Calculated by the Global Gasification Reaction and the Equation of Heat Balance on the Burning Surface

T_s, K	$\frac{dT}{dz}$, 10^6 K/m	q, cal/g	ΔQ, kal/g
687	3.55 [8]	121	123
633	4 [4]	95	116
593	7 [5]	133	170

$$+\int_{T_{\delta\to l}}^{T_s} c_{p,\mathrm{HMX}_l}(T)dT - q - q_r,$$

$$q = \lambda_g(T)\left(\frac{dT}{dz}\right)_{z=0}\Big/ m.$$

Here q and q_r are the heat transfer from the gas phase to the burning surface due to heat conduction and radiation, respectively, λ_g is the thermal conductivity of the gas phase, and m is the mass burning rate.

The calculations were performed for three values of T_s and their corresponding values of the temperature gradient and mass burning rate [4, 5, 8]. The composition of the gaseous products near the burning surface corresponds to that given in line 1 of Table 6. For each value of the surface temperature, the thermal conductivity $\lambda_g(T)$ was calculated. The heat transfer from the gas phase to the burning surface due to radiation (q_r) was ignored since, according to data [6], it is only 7 cal/g (≈4–7% of the heat transfer due to heat conduction from the gas phase). The calculation results are presented in Table 8. It is evident that the choice of the temperature dependence of the heat capacity of HMX also has a strong effect on the final calculation result. The maximum difference in the values of Q due to the spread in the values of the parameters used in the calculation is 56 cal/g.

The difference between the heat release values in the reaction layer of the condensed phase calculated by the global gasification reaction and by the equation of heat balance on the burning surface can be expressed by the formula

$$\Delta Q = \Delta_f H^0(\mathrm{HMX}_s) + q + q_r - \sum \nu_i H(B_i)_{T=T_s}.$$

It is evident that the quantity ΔQ, in contrast to the absolute values of Q, is not affected by the choice of the temperature dependence of the heat capacity of HMX but has a large value (Table 9). This discrepancy is apparently related to the error of determining both the gasification product composition and the heat transfer from the gas phase to the burning surface due to heat conduction (q). From Table 9, it is evident that the difference between the values of q reaches ≈40 cal/g. The last term in the expression for ΔQ is the sum of positive and negative numbers close in value, and, hence, even small variations in the stoichiometric coefficients can lead to a significant change in ΔQ. In [30], using RDX as an example, it has been shown that agreement between the values of Q determined by different methods can be achieved by modifying the measured composition of the combustion products within the determination error. For RDX, $\Delta Q \approx 90$ cal/g. However, for HMX combustion, because it was not possible to determine the concentrations of all species found near the burning surface and even not all species were identified, modifying the combustion product composition to obtain agreement between differently determined values of Q is meaningless until the concentrations of these products are determined. Among the products not determined quantitatively, we note s-triazine ($C_3H_3N_3$) and dicyan (C_2N_2) which have high positive enthalpies of formation: 225.9 and 309 kJ/mole [29], respectively. Accounting for the concentrations of these products, which are not considered in the heat balance on the burning surface, can considerably reduce the observed difference in the values of Q.

Estimation of the HMX Vapor Pressure in the Flame at a Pressure of 1 Atm

Using the data of Table 6, the HMX vapor pressure on the burning surface was calculated to be ≈34 torr. The same estimate can be obtained by a different method. In [39], based on an analysis of available literature data, the following equation for the pressure vapor above liquid HMX is proposed:

$$p = 10^{11.0\pm1.9}\exp[(-27{,}600 \pm 1000)/RT].$$

Here p is in torr, T in K, and R in cal/(mole·K). In [39], the HMX boiling point calculated by this equation at atmospheric pressure was 744 ± 37 K. Thus the maximum temperature of the HMX burning surface at atmospheric pressure ($T_s = 687$ K [8]) known from the literature is below the boiling point of liquid HMX.

The HMX vapor pressures at the minimum temperature (593 K) and maximum temperature (687 K) were estimated to be 7 and 164 torr, respectively. Taking into account the fraction of HMX evaporated from the burning surface to the gas phase (0.345), the obtained range is 2–57 torr. For HMX gasification in the combustion wave, the HMX vapor pressure (34 torr) calculated above is in this range. This agreement, however, can be accidental. Accounting for the error of determining

the parameters in the equation presented above for the equilibrium pressure of HMX vapor leads to a considerable spread in the values of the pressure vapor, which is several times larger than the absolute value of the pressure vapor obtained by MBMS.

Analysis of Mass Spectra of the HMX Gasification Products

In a mass spectrometric study [10] with an electron ionization energy of 22 eV, in addition to the main peaks, low-intensity peaks were recorded near the burning surface (the brutto formula of the presumed species is given in parentheses): 42 and 43 (HNCO), 45 (H_3NCO), 47 (HNO_2), 54 ($C_2H_2N_2$), 70 (H_2C_2NO), 81 ($H_3C_3N_3$), and 97 ($H_3C_3N_3O$). In our experiments (electron energy 70 eV) these peaks were also found in the mass spectra of the HMX gasification products during combustion. Therefore, it can be assumed that the species given above in parentheses are present near the HMX burning in both laser-assisted and self-sustained combustion. In addition, peaks 40, 41, 52, 56, 67, and 75 were found. Peaks 40, 41, and 67 were not identified. Presumed species were not considered in the flame structure calculations. Peaks 56 and 75 were identified as belonging to HMX vapor and were determined quantitatively. The intensity of mass peak 52 increases with increasing distance from the burning surface. Mass peak 52 is presumably identified as dicyan (C_2N_2).

At present, identification of all recorded peaks is impossible because of complex combustion chemistry and insufficient information on individual mass spectra of the species formed in nitramine flames.

CONCLUSIONS

The chemical structure of an HMX flame in air at a pressure of 1 atm was studied using molecular beam mass spectrometric sampling. The time scan of the species concentration profiles shows periodic pulsations due to variations in the HMX burning rate. HMX vapor is found near the burning surface. A total of 11 species were identified in the flame: H_2, H_2O, HCN, N_2, CO, CH_2O, NO, N_2O, CO_2, NO_2, and HMX vapor. The averaged flame structure of HMX, as well as that of RDX, has two main zones of chemical reactions. In the first zone ≈0.8 mm wide adjacent to the burning surface, HMX vapor decomposition and the reaction of NO_2, N_2O, and CH_2O with the formation HCN and NO take place. In the second zone ≈0.8–1.5 mm wide, HCN is oxidized by nitric oxide with the formation of the final combustion products. It is shown that, during HMX combustion at a pressure of 1 atm, thermodynamic equilibrium in the final flame zone (at a distance of 3 mm from the burning surface) is not reached. The global reaction of HMX gasification at a pressure of 1 atm was calculated from measured species concentration profiles near the burning surface. 35% of the HMX is evaporated from the burning surface to the gas phase. The calculations show that the heat release in the reaction layer of the HMX condensed phase obtained by the global gasification reaction far exceeds the heat release determined by the equation of heat balance on the burning surface using literature data on microthermocouple measurements. The data obtained can be used for the further improvement and validation of HMX combustion models.

This work was supported by the U.S. Army Research Office (Grant No. DAAD19–02-1-0373).

REFERENCES

1. O. P. Korobeinichev, L. V. Kuibida,and V. Zh. Madirbaev, "Investigation of the chemical structure of the HMX flame," *Combust., Expl., Shock Waves*, **20**, No. 3. 282–285 (1984).
2. L. V. Kuibida, "Investigation of the flame structure of nitramines using molecular beam mass spectrometric sampling," Candidate's Dissertation in Phys. and Math., Novosibirsk (1988).
3. O. P. Korobeinichev, L. V. Kuibida, A. A. Paletsky, and A. A. Chernov, "Study of solid propellant flame structure by mass spectrometric sampling," *Combust., Sci. and Technol.*, **113–114**, 557–571 (1996).
4. A. A. Zenin, "HMX and RDX: Combustion mechanism and influence on modern double-base propellant combustion," *J. Propuls. Power*, **11**, No. 4, 752–758 (1995).
5. A. A. Zenin, V. M. Puchkov, and S. V. Finyakov, "Characteristics of HMX combustion waves at various pressures and initial temperatures," *Combust., Expl., Shock Waves*, **34**, No. 2, 170–176 (1998).
6. A. Zenin and S. Finjakov, "Characteristics of octogen and hexogen combustion: A comparison," in: *Proc. of 37th Int. Annu. Conf. of ICT*, Fraunhofer Institut Chemische Technologie, Karlsruhe, Germany (2006), pp. 118.1–118.18.
7. N. Kubota and S. Sakamoto, "Combustion mechanism of HMX," *Propellants, Explosives, Pyrotechnics*, **14**, No. 1, 6–11 (1989).
8. V. P. Sinditskii, V. Y. Egorshev, and M. V. Berezin, "Study on combustion of new energetic nitramines," in: *Proc. of 32th Int. Annu. Conf. of ICT*, Fraunhofer Institut Chemische Technologie, Karlsruhe, Germany (2001), pp. 59.1–59.13.

9. T. P. Parr and D. M. Hanson-Parr, "Solid propellant flame structure," in: *Symp. Proc. of Materials Research Soc.*, Vol. 418, Pittsburgh (1996), pp. 207–219.
10. C.-J. Tang, Y. J. Lee, G. Kudva, and T. A. Litzinger, "A study of the gas-phase chemical structure during CO_2 laser assisted combustion of HMX," *Combust. Flame*, **117**, Nos. 1–2, 170–188 (1999).
11. T. Parr and D. Hanson-Parr, "Solid propellant flame chemistry and structure," in: K. Kuo and T. P. Parr (eds.), *Non-Intrusive Combustion Diagnostics*, Begell House, New York–Wallingford (1994), pp. 571–599.
12. T. Parr and D. Hanson-Parr, "Optical spectroscopic measurements of energetic material flame structure," in: *Overviews of Recent Research on Energetic Materials*, World Scientific Publ., Singapore (2005). (Advanced Series in Physical Chem., Vol. 16.)
13. G. Lengelle, J. Duterque, and J. F. Trubert, "Physicochemical mechanisms of solid propellant combustion, solid propellant chemistry," in: V. Yang, T. B. Brill, W.-Z. Ren (eds.), *Progress in Astronautic and Aeronautic*, Vol. 185: *Combustion, and Motor Interior Ballistics*, AIAA, Reston (2000), pp. 287–332.
14. T. Mitani and F. A. Williams, "A model for the deflagration of nitramines," in: *21th Symp.* (*Int.*) *on Combustion*, Combustion Inst., Pittsburgh (1986), pp. 1965–1974.
15. J. E. Davidson and M. W. Beckstead, "A three-phase model of HMX combustion," in: *26th Symp.* (*Int.*) *on Combustion*, Combustion Inst., Pittsburgh (1996), pp. 1989–1996.
16. V. N. Simonenko, A. B. Kiskin, V. E. Zarko, and A. G. Svit, "Special features of nitramine combustion at atmospheric pressure," *Combust., Expl., Shock Waves*, **33**, No. 6, 685–687 (1997).
17. V. N. Simonenko, V. E. Zarko, and A. B. Kiskin, "Characterization of self-sustaining combustion of cyclic nitramines," in: *Proc. of 29th Int. Annu. Conf. of ICT*, Fraunhofer Institut Chemische Technologie, Karlsruhe, Germany (1998), pp. 169.1–169.14.
18. T. L. Boggs, "The thermal behavior of cyclotrimethylenetrinitrate (RDX) and cyclotetramethylenetetranitrmine (HMX)," in: K. Kuo and M. Summerfield (eds.), *Progress in Astronautic and Aeronautic*, Vol. 90: *Fundamentals of Solid-Propellant Combustion*, Academic Press, New York (1984), pp. 121–175.
19. "HMX Propellant Research Group. The fundamental study of HMX composite propellant and its practical application," Tech. Report No. TR-875, National Aerospace Laboratory (1985).
20. N. E. Ermolin and V. E. Zarko, "Modeling of cyclic nitramine combustion (review)," *Combust., Expl., Shock Waves*, **34**, No. 5, 485–501 (1998).
21. T. B. Brill and R. I. Hiyoshi, "Pyrolysis of energetic materials in inert vs. reactive atmospheres," in: *Proc. of 32nd Int. Annu. Conf. of ICT*, Fraunhofer Institut Chemische Technologie, Karlsruhe, Germany (2001), pp. 14.1–14.12.
22. T. B. Brill, "Connecting molecular properties to decomposition, combustion and explosion trends," in: *Overviews of Recent Research on Energetic Materials*, Chapter 1, World Scientific Publ., Singapore (2005). (Advanced Series in Phys. Chem., Vol. 16.)
23. R. R. Bernecker and L. C. Smith, "On the products formed in the combustion of explosives. Freeze-out the water–gas reaction," *J. Phys. Chem.*, **71**, No. 8, 2381–2390 (1967).
24. O. P. Korobeinichev, "Study of energetic material combustion chemistry by probing mass spectrometry and modeling of flames," in: *Overviews of Recent Research on Energetic Materials*, Chapter 3, World Scientific Publ., Singapore (2005), pp. 75–103. (Advanced Series in Phys. Chem., Vol. 16.)
25. O. P. Korobeinichev, L. V. Kuibida, A. A. Paletsky, and A. G. Shmakov, "Molecular beam mass spectrometry to ammonium dinitramide combustion chemistry studies," *J. Propuls. Power*, **14**, No. 6, 991–1000 (1998).
26. A. A. Paletsky, O. P. Korobeinichev, A. G. Tereshchenko, E. N. Tereshchenko, and P. D. Polyakov, "Flame structure of HMX/GAP propellant at high pressure," in: 30*th Symp.* (*Int.*) *on Combustion*, Combustion Inst., Pittsburgh (2004), pp. 2105– 2112.
27. R. Jr. Behrens, "Identification of octahydro-1,3,5,7-tetranitro-1,3,5,7-tetrazocine (HMX) pyrolysis products by simultaneous thermogravimetric modulated beam mass spectrometry and time-of-flight velocity-spectra measurements," *Int. J. Chem. Kinet.*, **22**, 135–157 (1990).
28. V. R. Stepanov, A. A. Fedotov, A. N. Pavlov, and G. M. Nazin, "Mass spectrometric study of the elementary stages of thermal decomposition of cyclic nitramines," in: *Chemical Physics of Combustion and Explosion Processes*, Proc. IX Symp. on Combustion and Explosion (1989), p. 100–103.
29. *NIST Chemistry WebBook* (http://webbook.nist.gov/chemistry/).
30. E. N. Volkov, A. A. Paletsky, and O. P. Korobeinichev, "RDX flame structure at atmospheric pressure," *Combust., Expl., Shock Waves*, **44**, No. 1. 43–54 (2008).
31. T. B. Brill, "Multiphase chemistry considerations at the burning surface nitramine monopropellants," *J. Propuls. Power*, **11**, 740–751 (1995).
32. E. S. Kim, V. Yang, and Y.-C. Liau, "Modeling of HMX/GAP pseudo-propellant combustion," *Combust. Flame*, **131**, 227–245 (2002).

33. N. Kubota, "Survey of rocket propellants and their combustion characteristics," in: K. Kuo and M. Summerfield (eds.), *Progress in Astronautic and Aeronautic*, Vol. 90: *Fundamental of Solid Propellant Combustion*, Chapter 1, AIAA, New York (1984), pp. 1–52.
34. G. Krien, H. H. Licht, and J. Licht, "Thermochemische untersuchungen an nitraminen," *Thermochim. Acta*, **6**, No. 5, 465–472 (1973).
35. J. L. Lyman, Y.-C. Liau, and H. V. Brand, "Thermochemical functions for gas-phase, 1,3,5,7-tetranitro-1,3,5,7-tetraazacyclooctane (HMX), its condensed phases and its larger reaction products," *Combust. Flame*, **130**, 185–203 (2002).
36. R. J. Kee, F. M. Rupley, and J. A. Miller, "CHEMKIN-II: A Fortran chemical kinetics package for the analysis of gas phase chemical kinetics," Sandia National Laboratories Report No. SAND 89-8009B (1989).
37. A. A. Ulanovskii, B. L. Shmyrev, and Yu. N. Altykhov, "Universal tungsten–rhenium heat convertres in high-temperature thermometry," *Pribory*, **5**, No. 4–13 (2006).
38. P. G. Hall, "Thermal decomposition and phase transition in solid nitramines," *Trans. Faraday Soc.*, **67**, No. 578, Part 2, 556–562 (1971).
39. Yu. Ya. Maksimov, "Boiling point and enthalpy of evaporation of liquid RDX and HMX," *Zh. Fiz. Khim.*, **66**, No. 2, 540–542 (1992).
40. D. M. Hanson-Parr and T. P. Parr, "Thermal properties measurements of solid rocket propellant oxidizers and binder materials as a function of temperature," *J. Energetic Mater.*, **17**, No. 1, 1–48 (1999).
41. R. L. Shoemaker, J. A. Stark, and R. E. Taylor, "Thermophysical properties of propellants," *High Temperatures — High Pressures*, **17**, 429–435 (1985).